IOSR Journal of Applied Physics (IOSR-JAP)
e-ISSN: 2278-4861.Volume 7, Issue 3 Ver. III (May. - Jun. 2015), PP 26-41
www.iosrjournals.org

Detection of Brain Tumor in MRI Utilizing Supervised Neural Networks and Adaptive HSOFM Algorithm

Rabab Saadoon Abdoon [1], Loay Kadom Abood [2] and S.M. Ali [3]
[1] *Department of Physics - College of Science-University of Babylon-Iraq* [2]*Department of Computer Science- College of Science- University of Baghdad- Iraq,* [3]*Remote Sensing Unit - college of science - University of Baghdad- Iraq,*

Abstract: *Brain tumors are one of the major causes of death among people. The chances of survival can be increased if the tumor is detected correctly at its early stage. In this paper feed forward neural networks and Hierarchical Self Organization Feature Map, (HSOFM) algorithm were utilized to detect, isolate and extract the tumor region in brain MR images with and without contrast agent. Intensity in one trail; intensity and standard deviation in second trail and intensity and Gray Level Co-occurrence Matrix, (GLCM) features in the third one were implemented as input features to the feed forward neural network to classify the tumor class adequately. As well as, adaptive HSOFM which is an unsupervised neural network was utilized to cluster brain MR images in order to extract the tumor region depending on the images histogram in one experiment and based on the Fuzzy C-Mean clusters centers in another one. The results showed that the performance of HSOFM was promising compared with the supervised neural networks.*
Keywords: *Neural Networks, MRI, Brain Tumor, GLCM and HSOFM.*

I. Introduction

The MR brain image analysis is used to extract clinical information that would improve diagnosis and treatment of disease. Brain tumors are one of the most common brain diseases, so the detection and the isolation of brain tumors in MRI are very important in medical diagnosis [1]. Detection of tumors in MRI of brain is not an easy task when the tumor is overlapped with dense brain tissues. Despite numerous efforts and acceptable results in brain tumors segmentation, accurate and reproducible segmentation and characterization of abnormalities still a challenging task due to the varieties in tumor shapes, locations and the change in intensities of various types of tumors [2]. Since the MR images are formed from huge number of pixels, the segmentation process became computationally complex and needs efficient computer memory [3]. To overcome segmentation ambiguity, multi segmentation methods should be adopted [4 – 8]. The successful analysis of multi-dimensional images may be accomplished by utilizing several techniques: supervised or unsupervised segmentation methods. Artificial neural networks play an important role in segmentation and classification of MRI. In this work, artificial neural networks with both schemes of training supervised and un supervised.

II. Artificial Neural Networks (Anns)

Artificial Neural Network (ANN) is a powerful data modeling tool that is able to capture and represent complex input/output relationships. The motivation for the development of neural network technology stemmed from the desire to develop an artificial system that could perform intelligent tasks similar to those performed by the human brain. Neural networks resemble the human brain in two ways: they acquire knowledge through learning and store this knowledge within inter-neuron connection strengths known as synaptic weights. The true power and advantage of neural networks lie in their ability to represent both linear and nonlinear relationships and in their ability to learn these relationships directly from the data being modeled. Artificial neural networks are parallel networks of processing elements called neurons or nodes that simulate biological learning. Each node in an ANN is capable of performing elementary computations. Learning is achieved through the adaptation of weights assigned to the connections between nodes. It is most widely used in medical imaging as a classifier in which the weights are determined by using training data and the ANN is then used to segment new data, this scheme of training is called Supervised fashion. ANNs can also be used in an Unsupervised fashion as a clustering method [9].

The model of artificial neuron has three simple sets of rules: multiplication, summation and activation. At the entrance of the neuron, the inputs are weighted i.e. every input value is multiplied by an individual weight. In the middle section of the neuron is a sum function that sums all weighted inputs and bias. At the exit of the neuron, the sum of previously weighted inputs and bias is passing through an activation function which is called transfer function [10], see Figure (1).

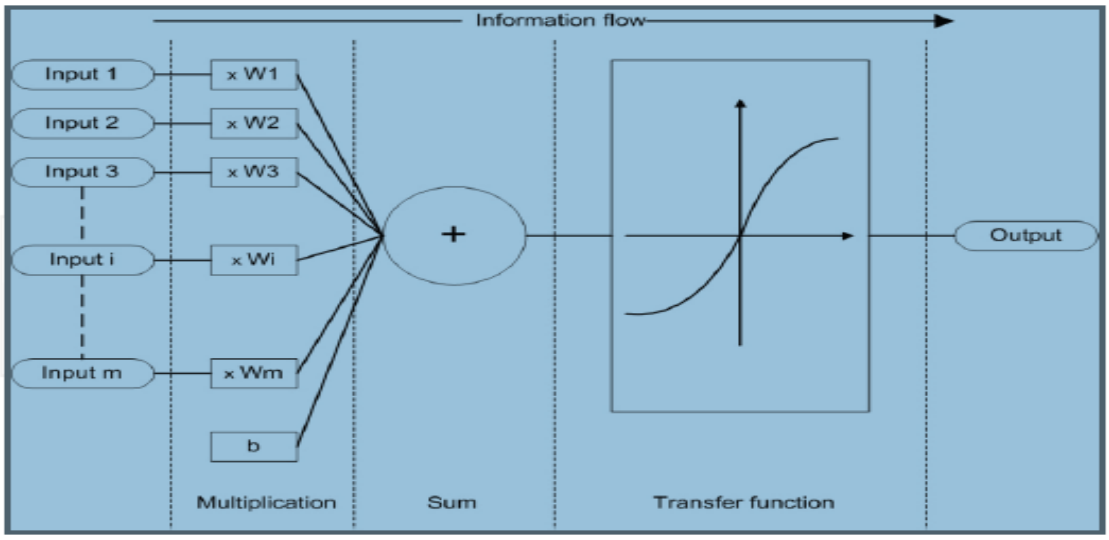

Figure (1): Working principle of an artificial neuron [10].

In artificial neuron, the information comes into the body of an artificial neuron via inputs that are weighted (each input can be individually multiplied with a weight). The body of the artificial neuron then sums the weighted inputs, bias and "processes" the sum with a transfer function. At the end, the artificial neuron passes the processed information via output(s). Benefit of artificial neuron model simplicity can be seen in its mathematical description below [10]:

$$y(k) = F(\sum_{i=0}^{m} w_i(k).x_i(k) + b) \qquad \ldots\ldots\ldots\ (1)$$

Where: $x_i(k)$ is input value(s) in discrete time k where i goes from 0 to m, m is the number of input features, $w_i(k)$ is weight value in discrete time k , k is bias, F is a transfer function, $y(k)$ is output value in discrete time k. It is selected on the basis of problem that artificial neural network needs to be solved and in most cases, it is one of the following set of functions: Step function, Linear function and Non-linear (Sigmoid) function .

When combining two or more artificial neurons, an artificial neural network is formed. If a single artificial neuron has almost no usefulness in solving real-life problems, the artificial neural networks have. The way that individual artificial neurons are interconnected is called architecture or topology. Figure (2) illustrates a simple example of feed forward architecture of neural network. By observing this figure, the individual neurons are grouped in layers for easier handling and mathematical description of an artificial neural network. Three layers can be seen: input, hidden and output layer.

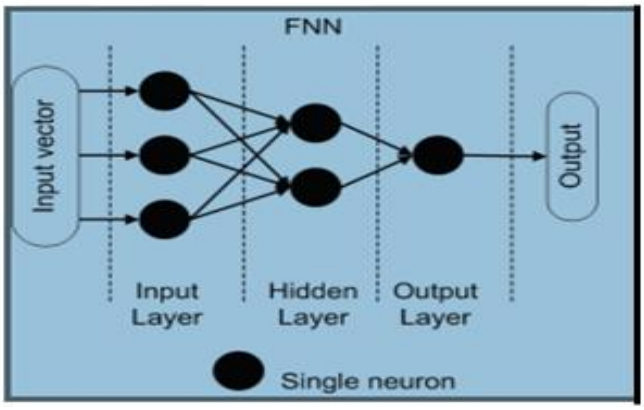

Figure (2): Feed-forward architecture of an artificial neural network [10].

After building the desired network, it has to learn proper response and this can be achieved through learning (supervised, un-supervised or reinforcement learning). No matter which method is being used, the task of learning is to set the values of weight and biases on basis of learning data to minimize the chosen cost function (activation function). The network function is determined largely by the connections between neurons. The neural network can be trained to perform a particular job by adjusting the values of the connections (weights) between neurons [11].

2.1 Artificial Neural Networks of Supervised Training Scheme

The neural networks are trained, so that a particular input leads to a specific target output (trained with supervised). Such a situation is shown in Figure (3). In this fashion, the network is adjusted based on a comparison of the output and the target until the network output matches the target. Typically, many such input/target pairs are used, in this supervised learning, to train a network [11].

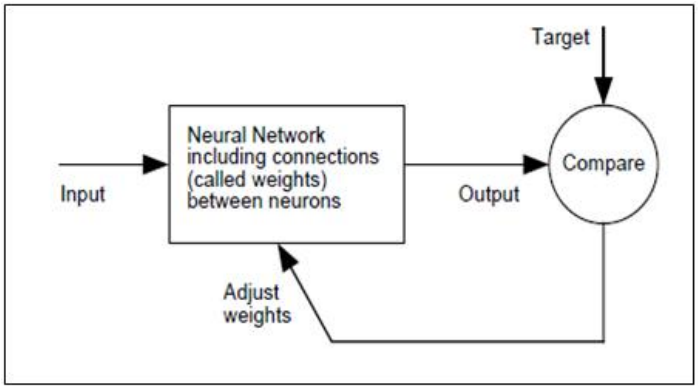

Figure (3): Supervised training of the Neural Network [11].

In this study many functions have been tested to achieve the classification task of MR brain images to detect and extract the tumor regions. It has been found that the following functions are the most adequate: the activation function of type Feed forward back propagation with training function of type Conjugate gradient back propagation with Fletcher-Reeves, learning function of type Gradient descent with momentum weight and bias learning function, and with transfer function of type Hyperbolic tangent sigmoid.

2.2 Artificial Neural Networks of Un-Supervised Training Scheme

In Un-supervised fashion of training, the network is trained for a specific data set and then adopting this stage to classify the test input data. Clustering operation is achieved by this type of neural networks. In clustering problems, the ANN clusters observations in two main stages. In the first, the learning rule is used to train the network for a specific data set. This is called training or learning stage. In the second, the observations are classified, which is called a recall stage. As mentioned before, the ANNs work into layers. The input layer contains the nodes through which data are input. The output layer generates the output that is interpreted by the user. Between these two layers there can be more layers (hidden layers). The output of each layer is an input of the next layer until the signal reaches the output layers as shown in Figure (4) [12].

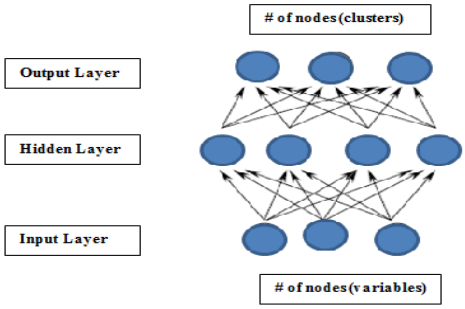

Figure (4): Illustration of a neural network for clustering [12].

One of the more important unsupervised ANN is the Self-Organization Feature Map (SOFM) or SOM that was proposed by Kohonen [13]. It is a feed-forward neural network that has been utilized for medical image segmentation. Self-organizing map is different in comparison to other artificial neural networks in the sense that they use a neighborhood function to preserve the topological properties of the input space [10]. The

procedure for placing a vector from data space onto the map is to find the node with the closest weight vector to the vector taken from data space and to assign the map coordinates of this node to this vector. Euclidean distance to all weight vectors is computed. The neuron with weight vector most similar to the input is called the Best Matching Unit (BMU). The weights of the BMU and neurons close to it in the SOFM lattice are adjusted towards the input vector. The magnitude of the change decreases with time and with distance from the BMU. The update formula for a neuron with weight vector [14]:

$$w_i(t+1) = w_i(t) + \alpha(t)h_{ci}(t)(x(t) - w_i(t)) \quad \ldots\ldots\ldots (2)$$

Where $w_i(t)$ indicates the weight assigned to input x_i , $\alpha(t)$ is a monotonically decreasing learning coefficient, and $h_{ci}(t)$ is the neighborhood function, typically considered as a Gaussian function. The process repeats for a large number of iterations. SOFM preserves the most important topological and metric relationships of the primary data items. SOFM is utilized for medical image segmentation [14, 15].

III. Grey Level Co-Occurrence Matrix Features

Texture is one of the most commonly used features to analyze and interpret images, specifically medical images. Texture is a measure of the variation of the intensity of a surface quantifying properties such as smoothness, coarseness, and regularity. It is often used as a region descriptor in image analysis and computer vision. Specifically, a textured region consists of a connected set of pixels that satisfy a given gray-level property which occurs repeatedly in an image region [16]. Several methods have been applied towards the analysis and characterization of texture within medical images. Among those mentioned, in texture analysis, two-dimensional dependence matrices (Co-occurrence Matrices) are extensively used, they are able to capture the spatial dependence of gray-levels which contributes to the perception of texture [16]. For details, see [17, 18, 19]. In this work, Contrast, Entropy, Homogeneity and Energy texture features were adopted as extra input features besides the intensity to investigate the performance of the adopted net.

IV. Experiments And Results

Many trails were achieved to fulfill the aim of this work utilizing many images from Hilla Surgical Hospital and Whole Brain Atlas Web Site.

4.1 Neural Networks of Supervised Training Scheme

Supervised Feed Foreword Neural Networks are used. Different architectures with different training algorithms were utilized. The first trail was carried out using one hidden layer network and conjugate gradient as well as Fletcher-Reeves as training algorithm. Training sets were extracted carefully from different slices for each brain tissue. Numbers of samples that have been utilized to train the network were equal to 650 for each class of the seven classes adopted in this scheme:. Background, Skull, CSF, GM, WM, Tumor without contrast agent and Tumor with contrast agent. Training was carried out with different hidden nodes number like 6, 8, 10, 12, 14, 16, 18 and 20. The histograms of the training datasets adopted for training the neural network are shown in Figure (5).

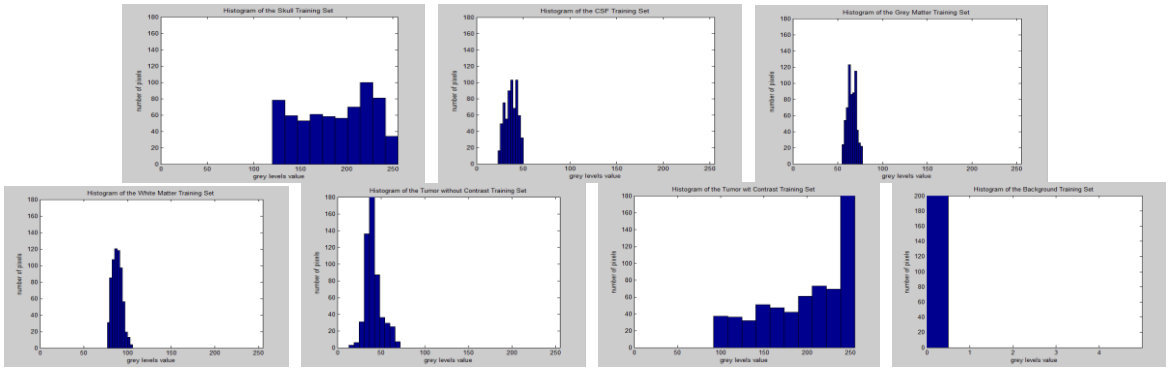

Figure (5): Histograms of the training datasets: Skull, CSF, GM, WM, Tumor without contrast, Tumor with contrast and Background from 1st one to the last respectively.
(The range for Background class 0-0.5).

The histograms of extracting training sets reveal that the spectrum overlapping is dominant which indicates that classes separation will be a very hard task.

4.1.1 Neural Networks of Supervised Training Scheme Utilizing Intensity

The adopted neural network was implemented to classify R3T1 image, that contains tumor without contrast agent, with different number of hidden nodes: 6, 8, 10, 12, 14, 16, 18, and 20. Figure (6) illustrates the results with number of hidden nodes: 6, 12, 18 and 20, from first one to the last one respectively as samples. First image of each one represents the classified image and the second one shows the seven classes of the corresponding classified image which are Background, Skull (bone), CSF, GM, WM, Tumor without contrast, Tumor with contrast and the eighth one represents the unclassified pixels for the membership values less than for example 0.4.

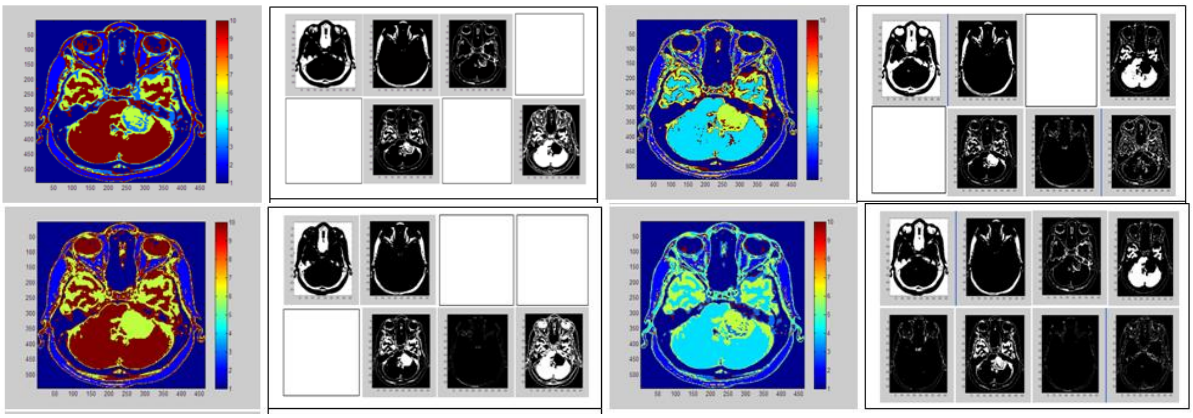

Figure (6): The resultant classified R3T1image by the adopting neural network of different number of nodes: 6, 12, 18 and 20 and its corresponding eight classes from first image to the last one.

The minimum number of unclassified pixels was found in the cases of 12 and 20 hidden nodes. The tumor regions of the tested image that was classified correctly as tumor without contrast utilizing the adopted network (with 6, 12, 18 and 20 hidden nodes), is extracted and demonstrated in Figure (7).

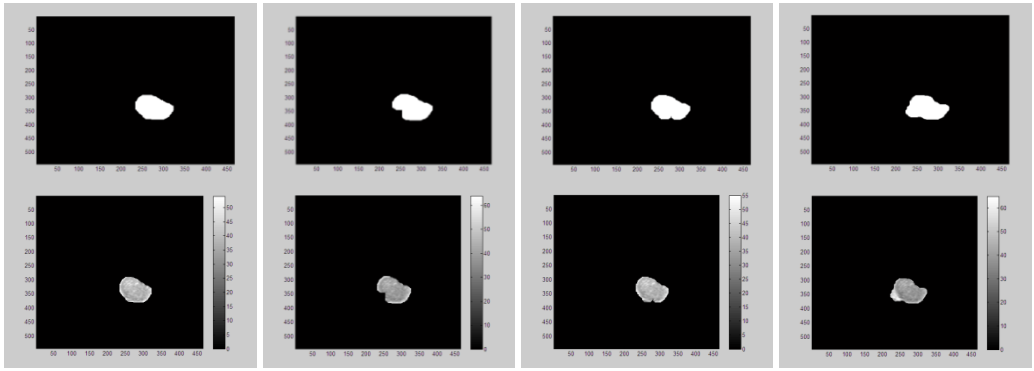

Figure (7): The tumor region BW and gray images that extracted utilizing the adopted neural network for the testing input image.

The tumor regions were extracted by selecting the class that the tumor seems to belong to, then applying many morphological opening processes with disk-shaped structuring element of radii 17, 15, 14 and 13 pixels for hidden nodes 6, 12, 18 and 20, respectively. In addition, some cases were needed to apply dilation to obtain the tumor region. The values of the calculated geometrical properties of these extracted tumor regions are presented in Table (1).

Table (1): The geometrical properties of the tumor region extracted from image R3T1 utilizing neural network of supervised training mode with different number of nodes in the hidden layer.(image size= 544×466 pixels).

Geometrical Properties	Number of Hidden Neurons (Nodes)			
	6	12	18	20
Area (Pixel)	6167	6416	6120	6542
Center of Mass Coordinates	337 275	336 277	337 275	341 270
Equivalent Diameter (pixel)	88.6119	90.3831	88.2736	91.2663
Perimeter (pixel)	356	380	382	382
Eccentricity	0	0	0.2085	0.5220

4.1.2 Neural Networks of Supervised Training Scheme Utilizing Intensity and Standard Deviation

As an adaptive procedure, Entropy and Standard deviation of the samples images were adopted in addition to the intensity as three input features instead of the intensity only. The results of this technique were not encouraging. As an alternative trial, intensity and entropy were adopted as two input features. The results of this step were not encouraging too. The last steps in this technique, standard deviation and intensity were adopted as two input features. After training the adopted network of one hidden layer with ten nodes, its training results were simulated to the test images which are: first one contains tumor without contrast agent named 3RT1 and a second contains tumor with contrast agent named M11T1. This technique was implemented with mean square error of the best validation of 0.073319 at epoch 438. The classified resultant images and their classes are illustrated in Figures (8) and (9) for the R3T1 and M11T1 images, respectively.

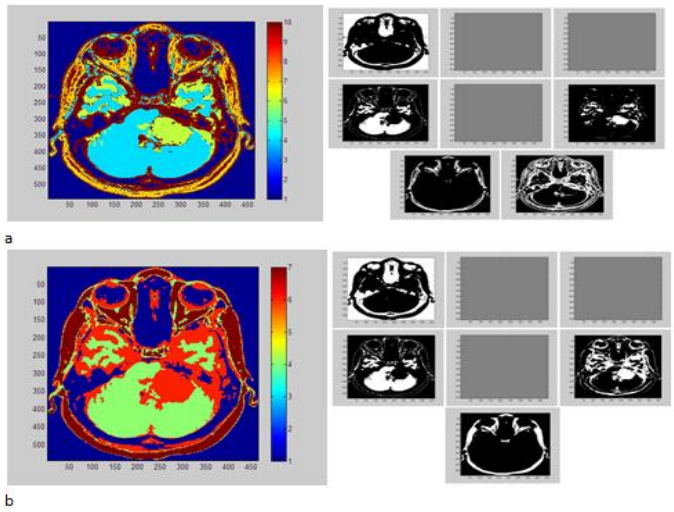

Figure (8): The resulted classified R3T1 image and its seven classes: Background, Skull, CSF, GM, WM, Tumor without contrast agent, and Tumor with contrast agent respectively, (a) with thresholding condition the last image for the unclassified pixels, and (b) without thresholding condition.

Tumor region is classified as tumor class in the two cases correctly but with small extra region that belongs to GM in case (a); and GM as well as extra pixels belonging to the eye's sockets in case (b) , as illustrated in Figure (8). These extra pixels can be removed by manipulating probability value i.e. thresholding, the probability leaves only high reliability one, case (a).

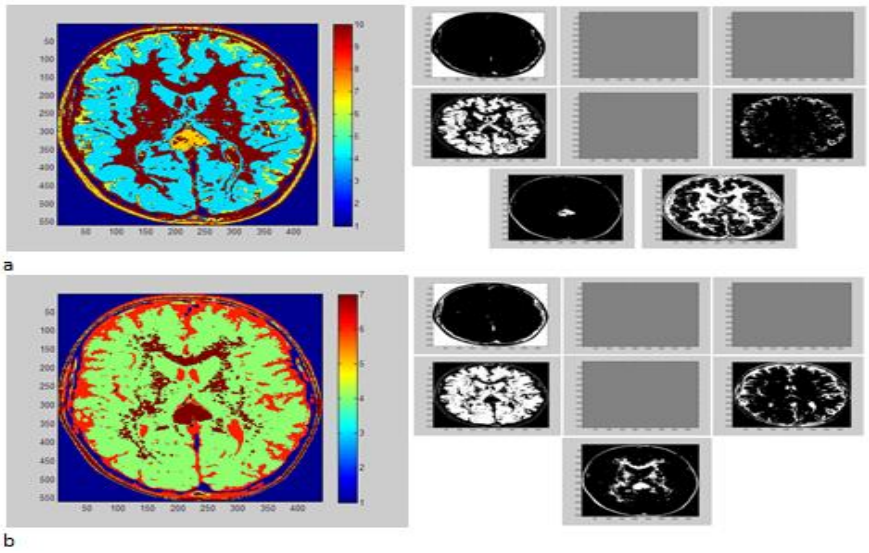

Figure (9): The resulted classified M11T1 image and its seven classes: Background, Skull, CSF, GM, WM, Tumor without contrast agent, and Tumor with contrast agent respectively, (a) with thresholding condition the last image for the unclassified pixels, and (b) without thresholding condition.

Observing Figure (9), tumor region is classified also as tumor class, as desired, but with extra pixels belonging to WM in case (b). These extra pixels can be removed by manipulating probability value as mentioned previously, the probability leaves only high reliability one, case (a).

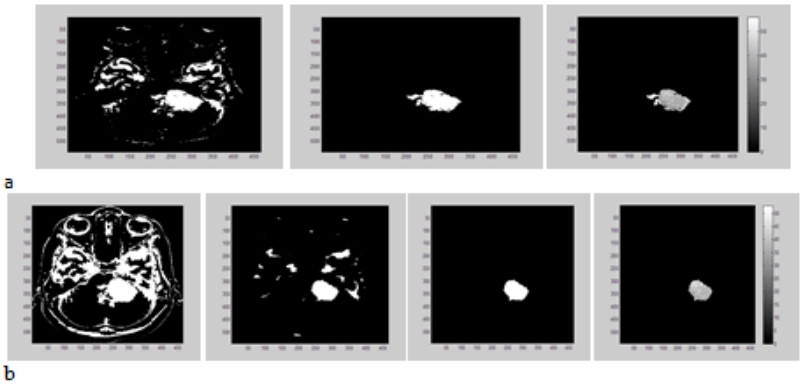

Figure (10): The steps of getting the gray level image of the extracted tumor from R3T1 image, (a) with thresholding condition, and (b) without thresholding condition.

Figure (10) a & b shows the steps of getting the tumor region from R3T1 image after applying morphological erosion process and regional area process that were utilized to select areas that exceed the specific pixels number. In (a), applying this process to extract the area that exceeds 2500 pixels, while in (b) applying erosion process with disk-shaped structuring element of radius equals six pixels to get rid of the weakly connected pixels and then applying regional area process to extract the area that exceeds 1300 pixels. Thresholding process is considered here as a substitute operator of morphology. Neural network response is a probabilistic rather than deterministic one, the reason that eliminating extra pixels could be achieved by selecting proper threshold value.

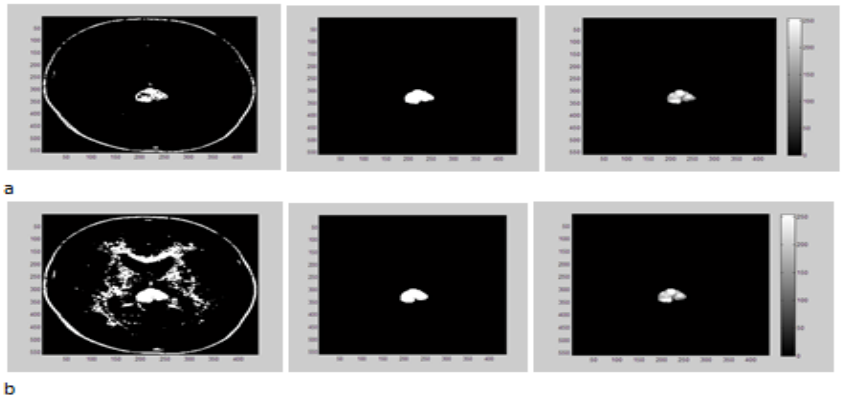

Figure (11): The steps of getting the gray level image of the extracted tumor from M11T1 image. (a)With thresholding condition, and (b) without thresholding condition.

Steps of getting the tumor region from M11T1 image are shown in Figure (11) a & b by applying morphological holes filling and opening process with disk-shaped structuring element of radius equals six pixels in (a) while in (b) opening process with disk-shaped structuring element of radius equals twelve pixels is needed. The values of the geometrical properties of the extracted tumor region from the images R3T1 and M11T1 with and without thresholding condition, by adopting this technique, were calculated and listed in Table (2).

Table (2): The values of the geometrical properties of the extracted tumor region for images R3T1 and M11T1 with and without thresholding condition. (R3T1 image size is 544×466 pixels and M11T1 image size is 558×440 pixels).

Image	State	Geometrical Properties				
		Mass(Area) (Pixel)	Center of Mass Coordinates	Equivalent Diameter (Pixel)	Perimeter (Pixel)	Eccentricity
R3T1	with Thresholding Condition	6147	336 269	88.4681	879	0.7239
	without Thresholding Condition	4605	336 276	76.5720	340	0
M11T1	with Thresholding Condition	2532	323 221	56.7789	248	0.4547
	without Thresholding Condition	2479	323 221	56.1815	256	0.4616

4.1.3 Neural Networks of Supervised Training Scheme Utilizing Intensity and GLCM Features

In order to investigate the dependency of performance quality on the extracted features, other features are extracted from training dataset like GLCM features which are: Contrast, Entropy, Homogeneity and Energy. A ten hidden nodes net were used in this experiment to classify M11T1 image. In this experiment, the method succeeded to isolate the tumor region, (see Figure (12)).

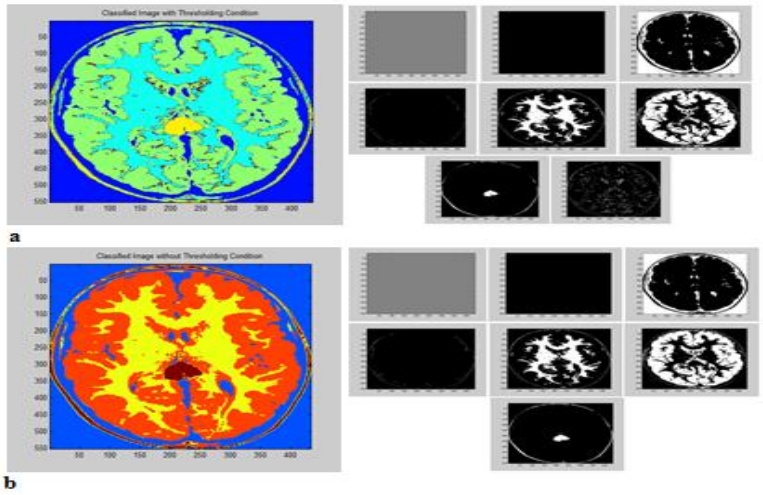

Figure (12): The resultant classified M11T1 image and its seven classes: Background, Skull, CSF, GM, WM, Tumor without contrast agent, and Tumor with contrast agent respectively by adopting intensity and GLCM features: (a) with thresholding Condition, and (b) without thresholding condition.

The steps of getting gray level image of the extracted tumor region of M11T1image is demonstrated in Figure (13).

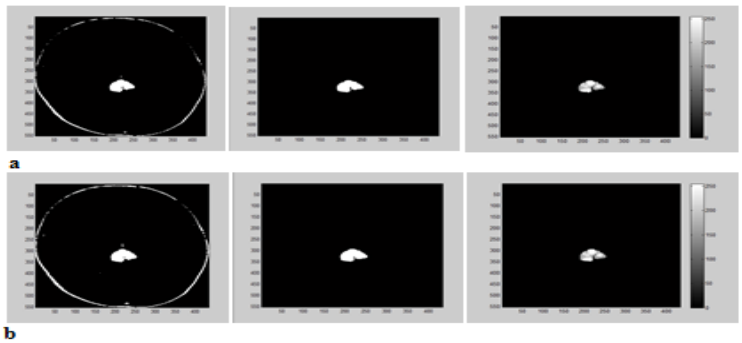

Figure (13): The steps of getting the gray level image of the extracted tumor from M11T1 image by adopting intensity and GLCM features, (a) with thresholding condition, and (b) without thresholding condition.

The only tumor region was extracted by applying morphological opening with disk-shaped structuring element of radius equals five pixels for (a) and six pixels for (b). The geometrical properties values of the extracted tumor region from image M11T1 with and without thresholding condition by adopting intensity and GLCM features were calculated and listed in Table (3).

Table (3): The geometrical properties values of the extracted tumor region from image M11T1 with and without thresholding condition, by adopting intensity and GLCM features. (Image size =552 x 434 pixels).

State	Geometrical Properties				
	Area (Pixel)	Center of Mass Coordinates	Equivalent Diameter(Pixel)	Perimeter (Pixel)	Eccentricity
with Thresholding Condition	2359	320 218	54.8049	270	0.4292
without Thresholding Condition	2439	320 218	55.7264	266	0.5114

4.2 Neural Networks of Unsupervised Training Scheme

An unsupervised training scheme neural networks were utilized to cluster and select the cluster to which the tumor region belongs. This task was achieved utilizing the Hierarchical Self Organization Feature Map. This clustering algorithm was implemented on four images named M9T, M10T1, M11T1 and U8T1 images shown in Figure (14), in many configurations.

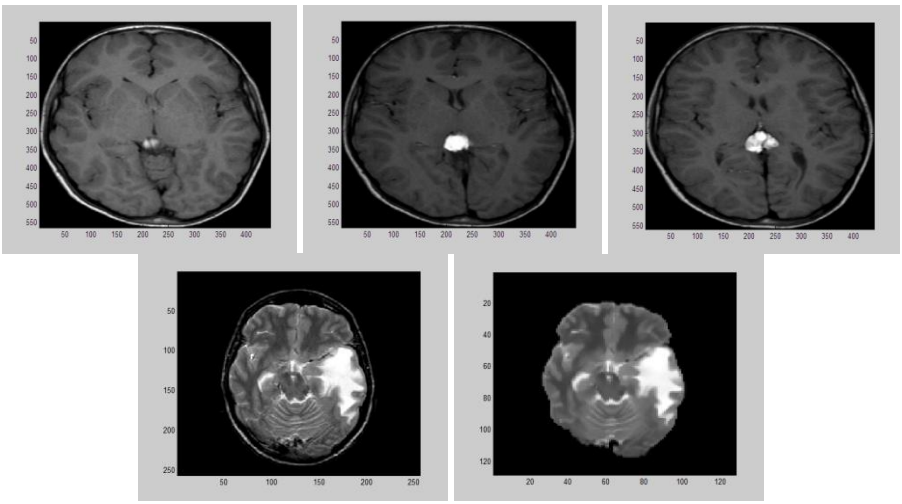

Figure (14): The original input images M9T1, M10T1, M11T1 in 1st row and U8T2 before and after skull stripping in the 2nd row.

In the first configuration, three major nodes with three sub nodes network architecture was used to segment M10T1 image and U8T2 image with and without skull. The initial weights of this network were taken by examining the images histogram and selecting the most distinct peaks rather than randomly. It can be shown from Figure (15) a & b that three major parts of the sliced image were collected which are: skull, WM and tumor in first part; GM, CSF and pixels that belong to the skull in the second part; while background and skull rounded pixels are found in the third part. For Figure (16) a & b, the three major parts are: the tumor region and pixels that belong to brain tissues in the first, GM and WM in the second; and background, CSF and pixels that belong to skull rounded tissues in the third part. In Figure (17) a & b of the skull stripped image, the three major parts are: brain matter (WM and GM) in first part; background and CSF in second and tumor region and CSF within the ventricle is found in the third part. Sub nodes were responsible for fine separation of each primary region. The final separation process was promising.

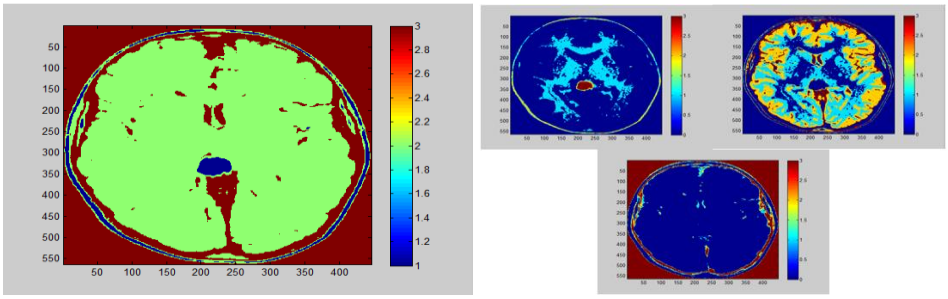

A

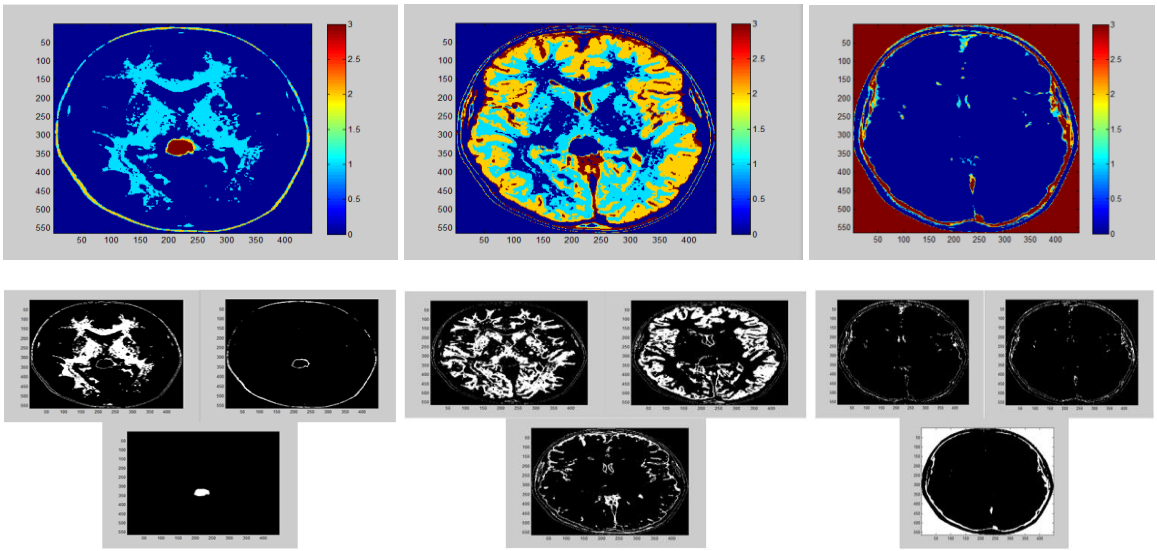

B

Figure (15): The results of implementing HSOFM with 100 iterations on M10T1 image.

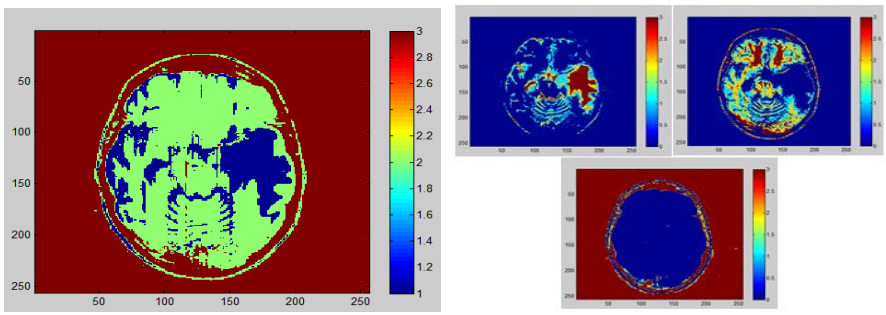

A

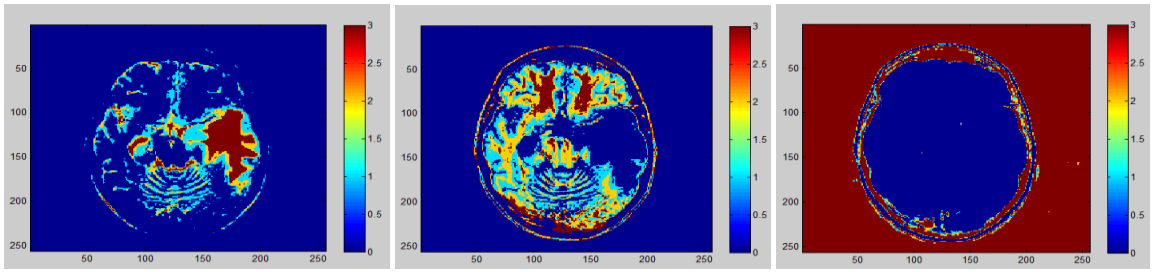

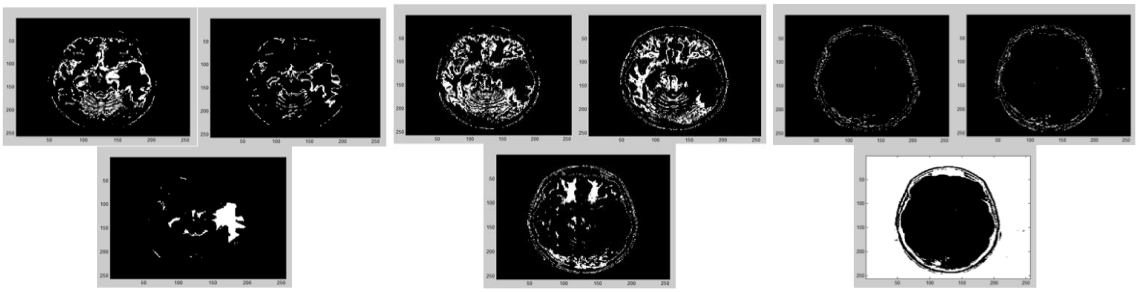

B

Figure (16): The results of implementing HSOFM with 100 iterations on U8T2 image before skull stripping.

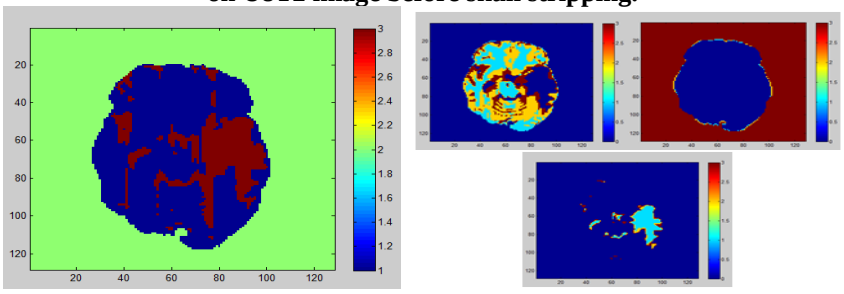

A

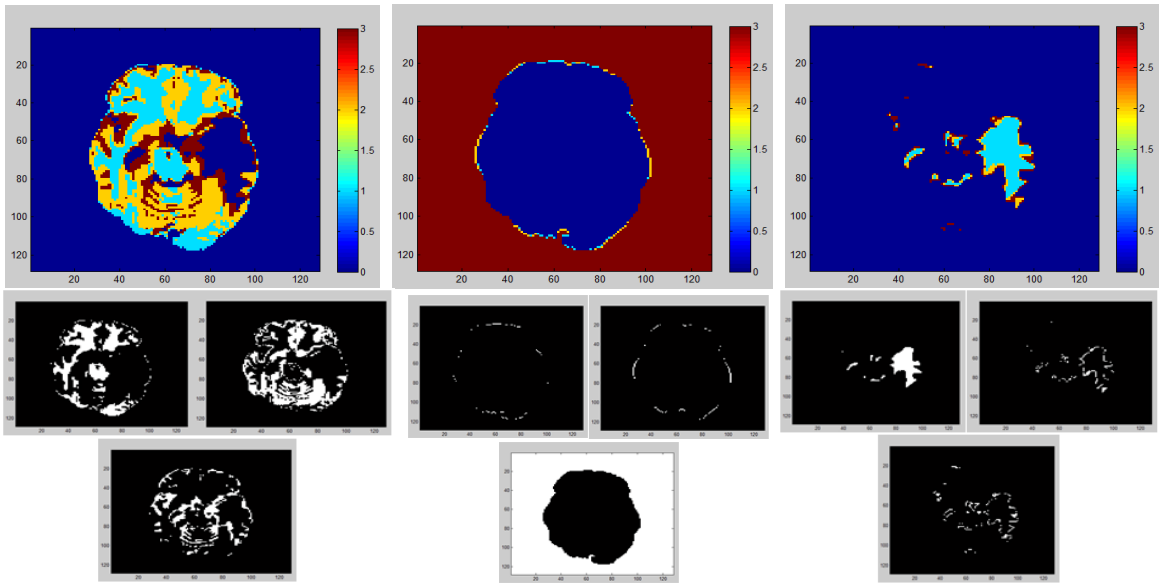

B

Figure (17): The results of implementing HSOFM with 100 iterations on U8T2 image after skull stripping.

In Figures (15), (16) and (17), part (a)shows the output image of the first stage and its three main segmented regions, while the subregions of each of those main regions are presented in (b) part. In another configuration, the number of nodes in the first stage was selected to be six in order to enforce the first three images in Figure (14) to cluster each of them into six regions, while in the second stage, each region is divided into three segments. The results of implementing this technique are illustrated in Figure (18).

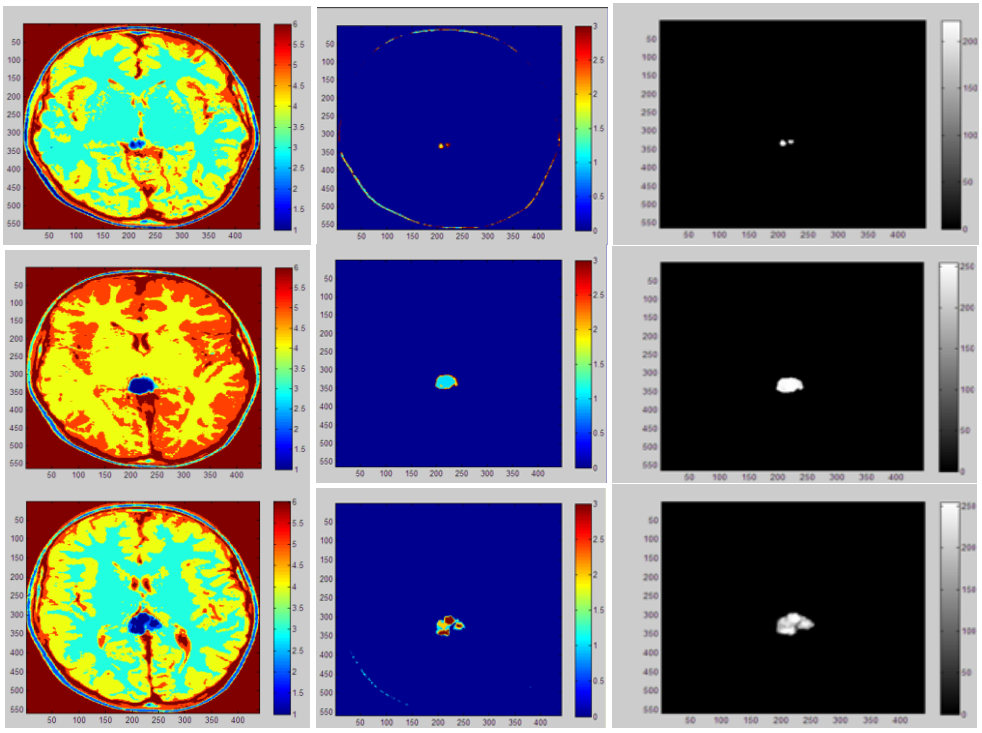

Figure (18): The results of implementing HSOFM algorithm on M9T1, M10T1 and M11T1 images. 1st column is the clustered image of 1st stage; 2nd column is the resultant tumor clustered image, and 3rd column is the gray image of the tumor.

Figure (18) illustrates the output results after 100 iterations. Extra process needed to clearly recover the tumor region. A morphological opening process with disk- shaped structuring element of radius 4, 1, and 2 pixels was used for images M9T1, M10T1 and M11T1, respectively. The small radius of this structure element reflects the high accuracy of the tumor isolation with small contribution of other classes. The last image needed an extra process because an extra refine region inside the tumor itself was separated, revealing the high distinction ability. Therefore, dilation process with 5 pixels structuring element radius was used to overcome this case. HSOFM succeeded to isolate the brain tumor correctly and clearly due to the proposed hierarchical arrangement according to the pre-knowledge of brain anatomy except very small traces depending on the slice sequence.

4.2.1 HSOFM Algorithm with Different Number of Iterations

HSOFM algorithm was implemented on M10T1 image with different number of iterations; 100, 200, 350, 500, 750 and 1000; and with six nodes in the primary stage and three sub nodes in the second stage. The calculated geometrical properties of the extracted tumor by implementing this technique are given in Table (4).

Table (4): The geometric properties of the tumor region extracted by implementing HSOFM algorithm on M10T1 image into six clusters, with different number of iterations. (Image size = 563x446 pixels).

Number of Iterations	Mass(Area) (pixel)	Center of Mass Coordinates	Perimeter (pixel)	Eccentricity
100	1452	332 219	178	0.4122
200	1461	332 219	178	0.4122
350	1898	331 220	202	0.4240
500	2089	331 221	220	0.4466
750	2089	331 221	220	0.4466
1000	2089	331 221	220	0.4466

4.2.2 HSOFM Algorithm with Different Number of Nodes

HSOFM algorithm was implemented on image M10T1 with different number of major nodes in the primary stage of this algorithm and with three sub nodes. The process is achieved with 500 iterations**.** The calculated geometrical properties of the tumor regions that were extracted by implementing this method are illustrated in Table (5).

Table (5): The geometric properties of the tumor region extracted by implementing HSOFM algorithm on M10T1 image with 500 iterations and with different number of nodes. (Image size = 563x446 pixels).

Number of Nodes	Mass(Area) (pixel)	Center of Mass Coordinates	Perimeter (pixel)	Eccentricity
5	2020	330 221	198	0.3379
6	2089	331 221	220	0.4466
7	2034	331 220	214	0.4166
8	2000	331 220	212	0.4542
9	1829	331 220	192	0.3919
10	1782	331 220	196	0.3445

By examining Tables (4) and (5) it can be deduced that, the best segmentation of this architecture is when using a net with (six nodes) and iterations (100-200) as shown in Table (4). So increasing iterations number may cause a negative response for learning. Increasing learning sometimes means information saturation, i.e. decreasing learning or information leakage (forgotten), besides that it means increasing computational time. Table (5) reveals another effect that the clusters number is a vital parameter also. So when the number of nodes becomes (9 or 10), the previous conclusion is proved, the iterations number in the second case was 500 iteration rather than 100 or 200. This can be attributed to the fact that, increasing number of nodes means increasing the storage capacity, since each node represents a storage unit, so more iterations number is needed to achieve the learning process.

4.2.3 HSOFM based on FCM Algorithm

As an adaptation of the HSOFM algorithm, HSOFM based on FCM is proposed. This algorithm was implemented on input images based on the centers values of the corresponding FCM clustered images. This technique was implemented on three images name M9T1, M10T1 and M11T1 to cluster them into six regions based on the centers values of the corresponding FCM clustered images as weights of the nodes links with 100 iterations. The results of this process are illustrated in Figure (19).

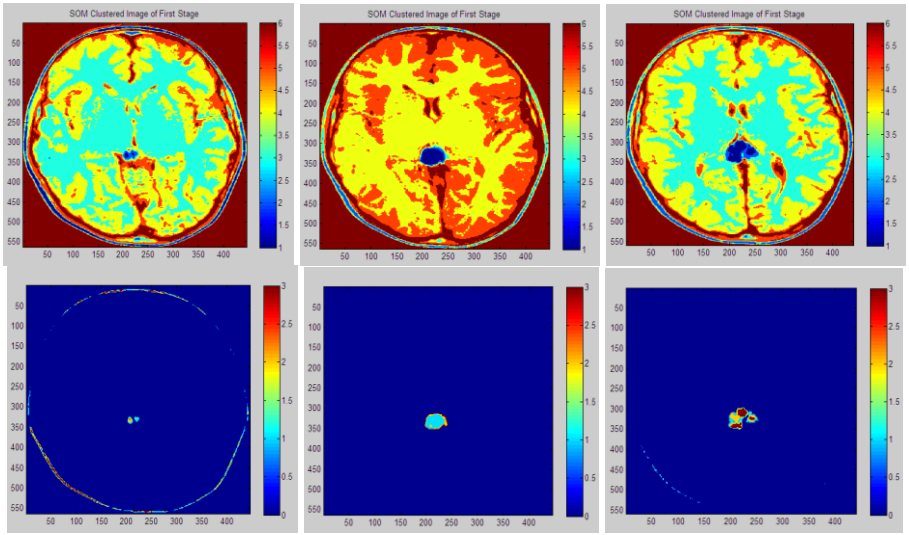

Figure (19): HSOFM results on images M9T1, M10T1 and M11T1 based on the centers values of the corresponding FCM clustered images (each images of size equals 563×446 pixels).

The opening morphological process is applied with disk-shaped structuring element of radius equals 4, 1, and 2 pixels for the three images, respectively. The extracted tumor region of M11T1 image needed more processing to recover the missed parts (pixels) and this is done by applying dilation process with disk-shaped structuring

element of radius equals 5 pixels. The tumor region images that resulted by implementing FCM algorithm of six clusters on M9T1, M10T1 and M11T1 images are shown in the first row of Figure (20), while the tumor regions images that resulted by implementing HSOFM based on FCM are demonstrated in the second row of Figure (20).

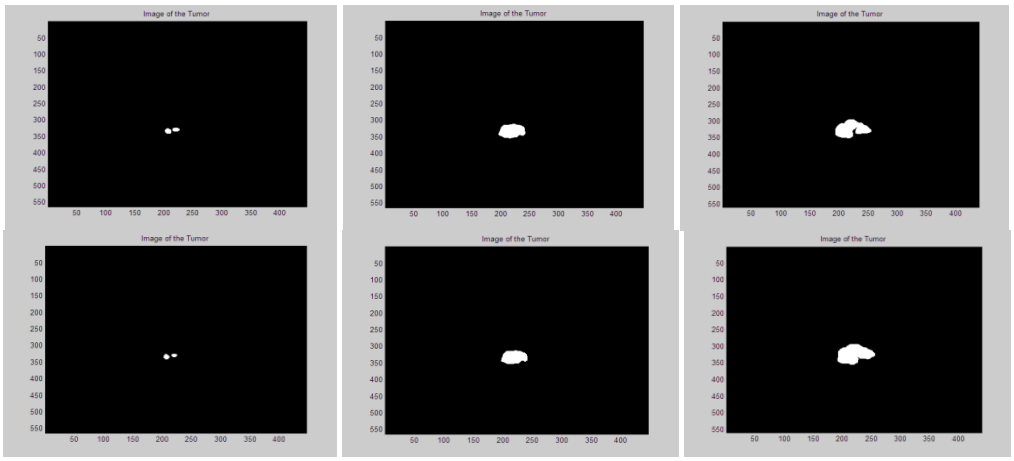

Figure (20): The extracted tumor regions by implementing FCM algorithm and HSOFM algorithm based on FCM on M9T1, M10T1 and M11T1 images.

To study the effect of the iterations number on the performance of this adaptive technique, it was implemented on M10T1 image with six clusters for different number of iterations: 100, 200, 350, 500, 750 and 1000. The calculated geometric properties of the extracted tumor region are presented in Table (6).

Table (6): Illustrates a comparison of the geometric properties of the tumor region that extracted by implementing HSOFM algorithm on M10T1 image into six clusters, based on the FCM algorithm cluster centers' values for different number of iterations. (Image size= 563x446 pixels).

Number of Iterations	Mass(Area) (pixel)	Center of Mass Coordinates	Equivalent Diameter (pixel)	Perimeter (pixel)	Eccentricity
100	1452	332 219	42.9970	178	0.4122
200	1461	332 219	43.1301	178	0.4122
350	1898	331 220	49.1590	202	0.4240
500	2089	331 221	51.5732	220	0.4466
750	2089	331 221	51.5732	220	0.4466
1000	2089	331 221	51.5732	220	0.4466

Table (6) reveals that the results of implementing HSOFM based on FCM seem to be very similar to conventional HSOFM (see Table (4)), i.e. there is no significant changes using this adaptation in segmentation. The improvement here is with the processing time, which is nearly half that is needed in HSOFM. In order to compare the various methods (FCM; HSOFM and HSOFM based on FCM), Table (7) illustrates the quantitative values for the tumor region for different image slices and with 100 iterations. Clearly the tumor area is so similar except when the morphological structuring element radius is large. The main goal is to separate the tumor region not the tumor area value.

Table (7): Illustrates the values of the geometrical measurements of the extracted tumor region of the images M9T1, M10T1 and M11T1, by implementing the clustering algorithms of six clusters: FCM; HSOFM and HSOFM based on FCM.

Geometrical Properties	FCM			HSOFM				HSOFM based on FCM			
	M9T1	M10T1	M11T1	M9T1	M10T1	M11T1		M9T1	M10T1	M11T1	
Mass(Area) (pixel)	277	1588	2160	207	1452	1698*	2687**	207	1452	1698*	2687**
Center of Mass Coordinates	331 213	332 219	323 221	331 212	332 219	323 219	323 220	331 212	332 219	323 219	323 220
Equivalent Diameter(pixel)	18.7800	44.9656	52.4423	16.2346	42.9970	46.4969	58.4910	16.2345	42.9970	46.4969	58.4910
Perimeter (pixel)	96	184	282	86	178	299	268	86	178	299	268
Eccentricity	0.7332	0.4037	0.3997	0.7581	0.4122	0.1898	0.1775	0.7581	0.4122	0.1898	0.1775

*This column for extracted tumor region utilizing opening morphological process. ** This column for extracted tumor region utilizing opening morphological process followed by dilation process.

V. Conclusions

The results showed that the performance of HSOFM is promising compared with the supervised neural networks. HSOFM succeeded to isolate the brain tumor correctly and clearly due to the proposed hierarchical arrangement according to the pre-knowledge of brain anatomy except very small traces depending on the slice sequence. Increasing clusters number is a positive factor but it is a constrained one i.e. there is an optimal number, less or more than this number will affect the performance. It can be also concluded that increasing clusters number (increasing main nodes) will increase the probability of extracting tumor pixels as large as possible; then this area begins to decrease as clusters increase. This behavior can be explained as follows: increasing clusters number, tumor pixels will be distributed on more than one cluster, (especially if it is known that tumor region has intensity variation). From the results, it is concluded that such network with, increased number of nodes, needs to be trained correctly by allowing the net to extract as large information as possible by increasing iterations number. A suitable iterations number depends mainly on the net structure as well as on the training vectors. Other parameters may affect the training like learning rate and neighborhood radius (number of nodes contribute learn each time). The results of implementing HSOFM based on FCM seem to be very similar to conventional HSOFM , i.e. there is no significant changes using this adaptation in segmentation. The improvement here is with the processing time, which is nearly half that is needed in HSOFM.

References

[1]. Toga W. A., Thompson P. M., Mega M. S., Narr K. L. and Blanton R. E., "Probabilistic Approaches for AtlasingNormal and Disease-specific Brain Variability", Anatomy and Embryology, Vol.204, No.4, PP. 267–282, 2001.

[2]. Khotanlou H., "3D Brain Tumors and Internal Brain Structures Segmentation in MR Images", Ph. D. thesis in signal and images, ENST, TELECOM Paris Tech, 2008.

[3]. Amir EhsanLashkari, "A Neural Network-Based Method for Brain Abnormality Detection in MR Images Using Zernike Moments and Geometric Moments", International Journal of Computer Applications, Vol. 4, No.7, PP.1-8, 2010.

[4]. Vannier M.W., Butterfield R. L., Jordan D., Murphy W. A., Levitt R. G. andGado M., "Multispectral Analysis of Magnetic Resonance Images", Radiology, Vol. 154, PP. 221–224, 1985.

[5]. Vannier M., Pilgram T., Speidel C., Neumann L., Rickman D. and Schertz L., "Validation of Magnetic Resonance Imaging (MRI) Multispectral Tissue Classification", Comp. Med. Imag. Graph.,Vol. 15, PP.217–228, 1991.

[6]. Ozkan M., Dawant B. M.and Maciunas R. J., "Neural-Network-based Segmentation of Muliti-Modal Medical Images: A Comparative and Prospective Study," IEEE Trans. Med. Imag., Vol. 12, PP. 534–544, 1993.

[7]. Taxt T. and Lundervold A., "Multispectral Analysis of the Brain using Magnetic Resonance Imaging", IEEE Trans. Med. Imag., Vol. 13, PP.470– 481, 1994.

[8]. Chang C. I. and Brumbley C., "A KalmanFiltering Approach to Multispectral Image Classification and Detection of Changes in Signature Abundance", IEEE Trans. Aerosp. Electron. Syst.,Vol. 37,PP. 257–268, 1999.

[9]. Reddick W.E., Glass J.O. and Cook E.N., "Automated Segmentation and Classification of Multispectral Magnetic Resonance Images of Brain using Artificial Neural Networks", IEEE Trans Med Imaging,16, PP.911–918, 1997.

[10]. Andrej Krenker , JanezBešter and Andrej Kos, "Introduction to the Artificial Neural Networks, Artificial Neural Networks-Methodological Advances and Biomedical Applications", Prof. Kenji Suzuki (Ed.), ISBN: 978-953-307-243-2, InTech, 2011..

[11]. Howard Demuth and Mark Beale,"Neural Network Toolbox For Use with MATLAB", User's Guide, Version 4, Neural Network Toolbox User's Guide, COPYRIGHT by The MathWorks, Inc, 2002.

[12]. Sueli A. Mingoti and Joab O. Lima, "Comparison SOM Neural Network with Fuzzy C-Means, K-Means and Traditional Hierarchical Clustering Algorithms", European Journal of Operational Research, 17, PP.1742-1759, 2006.

[13]. Kohonen T., "Self-Organization and Associative Memory", Springer-Verlag, New York, 1989.

[14]. Logeswari T. and Karnan M., "An Improved Implementation of Brain Tumor Detection using Segmentation based on Soft Computing", Journal of Cancer Research and Experimental Oncology Vol. 2, No.1,PP. 006-014, 2010.

[15]. MostafaJabaroutiMoghaddam and Hamid Soltanian-Zadeh, "Medical Image Segmentation Using Artificial Neural Networks, Artificial Neural Networks- Methodological Advances and Biomedical Applications", Prof. Kenji Suzuki (Ed.), ISBN: 978-953-307-243-2, InTech, 2011.

[16]. Chang K.I., Bowyer K.W. and Sivagurunath M., "Evaluation of Texture Segmentation Algorithms", IEEE Conf. on Computer Vision and Pattern Recognition Vol.1, No.21, PP. 294–299, 1999.

[17]. Haralick R.M., Shanmugam K. and Dinstein I., "Textural Features for Image Classification", IEEE Trans. on Systems, Man, and Cybernetics, Vol. Smc-3, No.6, PP. 610-621, 1973.
[18]. Conners R and Harlow C., "A Theoretical Comparison of Texture Algorithms", IEEE Transactions on Pattern Analysis and Machine Intelligence Vol.2, No. 3, PP.204–222, 1980.
[19]. Al Mutaz M. Abdalla, Safaai Dress and NazarZaki, "Detection of Masses in Digital Mammogram Using Second Order Statistics and Artificial Neural Network", International Journal of Computer Science & Information Technology (IJCSIT), Vol. 3, No. 3, PP. 176-186, 2011.